Stable Photoemission from the Wehnelt Aperture Surface in 4D Ultrafast Electron Microscopy

Simon A. Willis^{1,2}, David J. Flannigan^{1,2*}

- ^{1.} Department of Chemical Engineering and Materials Science, University of Minnesota, Minneapolis, MN, United States.
- ² Minnesota Institute of Ultrafast Science, University of Minnesota, Minneapolis, MN, United States.
- * Corresponding author: flan0076@umn.edu

Laser-based femtosecond (fs) transmission electron microscopy (TEM), dubbed 4D ultrafast electron microscopy (4D-UEM), consists of coupling a fs pulsed laser with a TEM [1-3]. Experiments are conducted in a stroboscopic pump-and-probe manner in order to study chemical and materials dynamics with picosecond to fs resolution [4-6]. Typically, fs ultraviolet (UV) laser pulses are trained on an electron source in the gun region, and discrete packets of photoelectrons are generated via the photoelectric effect. Though configurations and requirements vary, base TEMs equipped with (S)FEGs and TEGs can be operated as fs laser-based UEMs [7-9]. Owing to relatively low beam currents and to temporal structuring, pulsed-beam TEM has also been shown to mitigate specimen damage [10,11]. However, as is the case for conventional operation, oft-used electron source materials are inherently unstable under photo-illumination over long periods [9,12]. This poses challenges for long-time acquisitions seeking to monitor signal-intensity variations as an indicator of time-dependent structural changes. Perhaps even more detrimental is the resulting variation in electron-packet temporal duration and coherence during acquisition of both single data points and entire data sets. Here we show that photoemission with high long-term stability that is immediate and robust can be generated from the surface of the Wehnelt aperture in a TEG-based UEM. Further, we show that the resulting photobeam quality can be at least as good as that from LaB₆, whether under photo or thermionic operation. We hypothesize that the energy distribution and the temporal properties of the beam are improved relative to LaB₆ owing to the closer match of photon energy to aperture work function.

Comparison of photoemission stability and performance was done using two configurations. The first was a conventional on-axis configuration using a custom blunted, 0.1-mm diameter LaB₆ tip encircled with a graphite sheath. For this configuration, photoemission was carried out below the thermionic threshold at a heat-to value of either 0 or 20. The second was an unconventional off-axis configuration using the surface of the Ni Wehnelt aperture (0.5-mm diameter). Positioning of fs UV laser pulses (250 fs fwhm, 4.8 eV photon energy, estimated spot size of 50 µm fwhm) was done using a piezoelectric mirror mount housed in the probe periscope of the Tecnai Femto UEM. Experiments were done with laser pulses either entirely on the LaB₆ or entirely on the Wehnelt aperture surface. Figure 1 summarizes the results of the stability experiments. Figure 1a shows the stability of LaB₆ photoemission immediately after reducing the heat-to value from that which thermionic emission is observed and the source is saturated. The t = 0 position marks the moment when the lower heat-to value was reached, and photoemission was started. Both values tested display a biexponential decay. The heat-to 20 setting is relatively more stable than the heat-to 0 setting, decaying by 40% in the first 30 minutes compared to 95%, respectively. Photoemission current at heat-to 20 continued to steadily decline up to 320 minutes (where the measurement was stopped). The behavior is attributed to adsorption of gaseous species on the LaB₆ surface during cooling, following a Hertz-Knudsen-type behavior, and a resulting increase in work function. By comparison, photoemission from the aperture surface was significantly more stable for measurement times up to 70 minutes (note that this stability persists for much longer times), with a

standard deviation of only 1.0% (Fig. 1b). Aperture-photoemission stability is also immediate and robust, as demonstrated with a laser shuttering experiment (Fig. 1c). Photoemission current is immediately at its steady-state value upon unshuttering, remains stable for the duration of the measurement, and quantitatively repeats this behavior for several shuttering/unshuttering cycles. We attribute the difference in behavior between the LaB₆ and the Ni aperture to differences in work function (roughly a factor of two larger for Ni) and to the impact on adsorption of surface species.

Owing to the unconventional off-axis configuration of aperture photoemission, we conducted beam quality experiments (Fig. 2). Specifically, we compared the optimum beam size in Nanoprobe mode for LaB₆ and aperture photoemission, as well as for conventional thermionic emission from the same LaB₆ source (Fig. 2a-d). We also collected PBED and CBED patterns from 1T-TaS₂ and Si, respectively, using aperture photoemission (Fig. 2e,f). The optimized probe size measured at the detector for aperture photoemission was 19.7 nm fwhm, which was approximately the same as that for optimized conventional and photoemission from the 0.1-mm diameter LaB₆. The spot shape for aperture photoemission was nearly symmetric, as determined by peak fitting differently oriented line profiles. Quality of the diffraction patterns generated using aperture photoemission was also found to be acceptable. For PBED, first- and second-order satellite spots of the nearly commensurate chargedensity-wave (NCCDW) phase of 1T-TaS2 were resolved (Fig. 2e), while HOLZ rings from Si were resolved for CBED (Fig. 2f). This indicates that photobeam quality from a Ni Wehnelt aperture surface is at least as good as that from LaB₆, while the stability is significantly improved. We note that the number of electrons per packet (~hundreds) are intriguing with respect to conducting high-resolution UEM imaging [13], and the close match of UV photon energy to work function may lead to a relatively narrow energy distribution, though direct measurements are needed, as has been done with photoemission from the extractor in a FEG-based UEM [14,15].

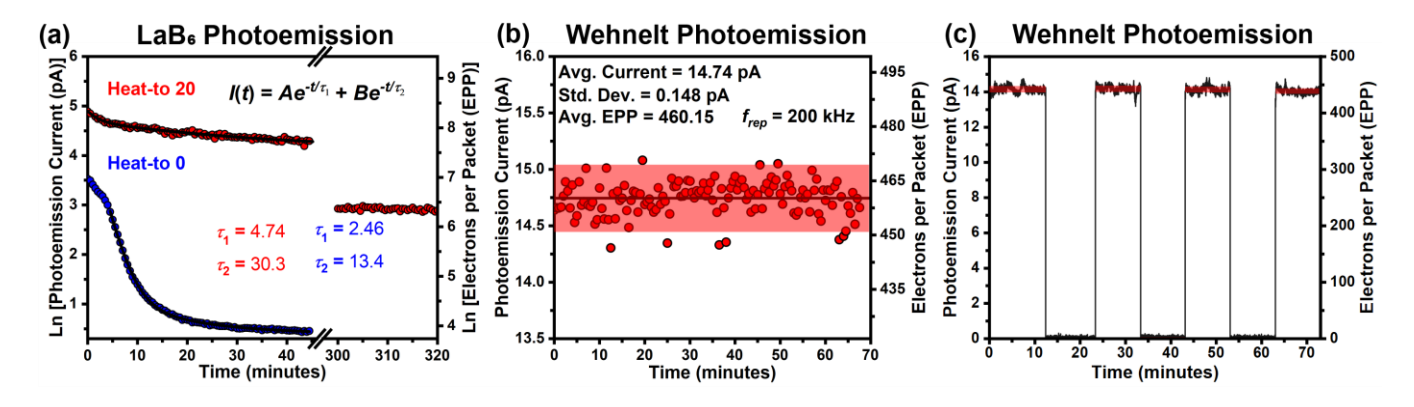


Figure 1. Photoemission stability from LaB₆ and a Ni Wehnelt aperture. (a) LaB₆ photoemission stability for heat-to values of 0 (blue) and 20 (red), both of which are below the thermionic threshold. The heat-to 20 data is the average of three separate trials, while the heat-to 0 data is the average of two trials. Each curve is fit with a biexponential decay function, and the time constants for both heat-to values are shown. Truncated longer-time data for the heat-to 20 setting is also shown. (b) Ni Wehnelt aperture photoemission stability over a 70-minute period. One standard deviation is 1.0%; the red band indicates two standard deviations from the average. The UV laser repetition rate (f_{rep}) was 200 kHz. (c) Immediacy and robustness of aperture photoemission stability via UV laser shuttering/unshuttering. The red bands indicate two standard deviations from the average.

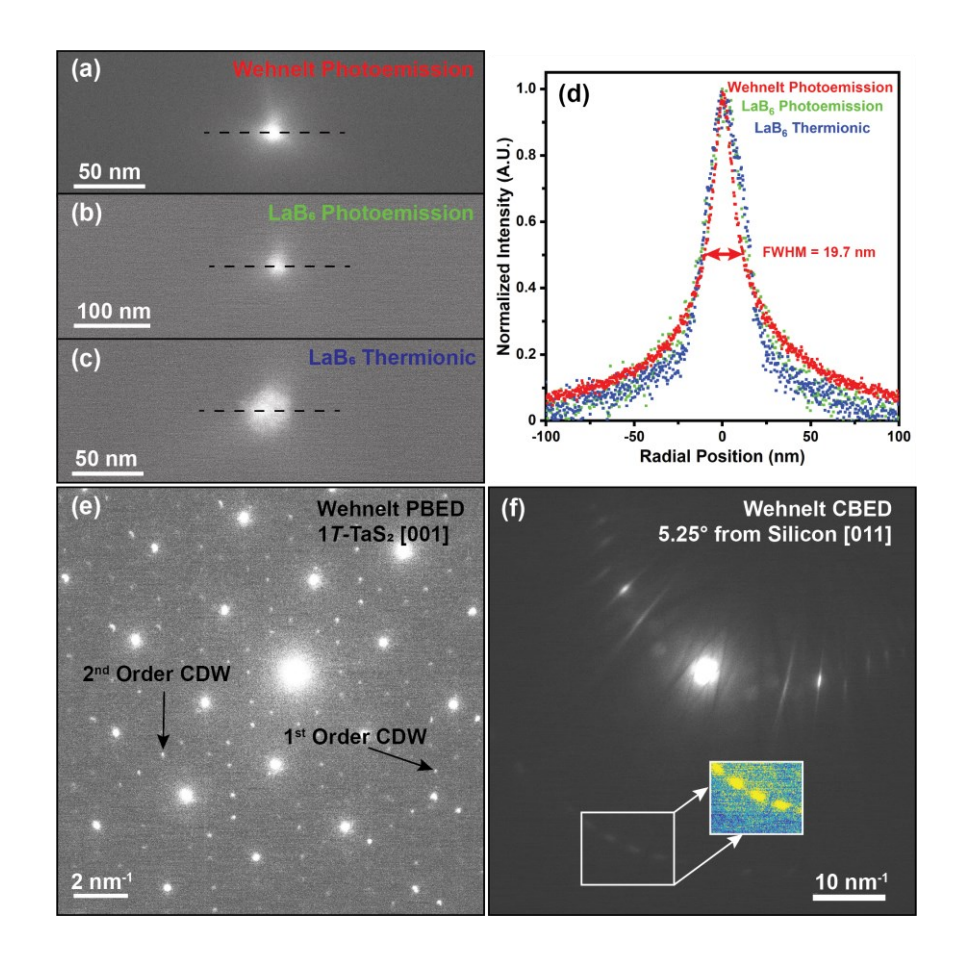


Figure 2. Beam quality for Wehnelt aperture photoemission. Beam spot size optimized in Nanoprobe mode for (a) aperture photoemission, (b) for LaB₆ photoemission, and (c) for thermionic emission from the same LaB₆ source. Dashed horizontal lines mark the positions at which line profiles were generated, as shown (normalized) in (d). All spots were roughly symmetric and of the same fwhm (20 nm). (e) PBED pattern of the [001] zone axis of the NCCDW phase of 1T-TaS₂ acquired with a camera length of 1.2 meters. Select first- and second-order CDW satellite spots are labeled. (f) CBED pattern of Si oriented at an α -tilt angle of 5.25° from the [011] zone axis. HOLZ rings are highlighted and false colored. The camera length was 0.285 m.

References:

- [1] A. H. Zewail, Science **328** (2010), p. 187. doi:10.1126/science.1166135
- [2] D. J. Flannigan and A. H. Zewail, Acc. Chem. Res. 45 (2012), p. 1828. doi:10.1021/ar3001684
- [3] D. A. Plemmons et al., Chem. Mater. 27 (2015), p. 3178. doi:10.1021/acs.chemmater.5b00433
- [4] D. R. Cremons et al., Nat. Commun. 7 (2016), 11230. doi:10.1038/ncomms11230
- [5] S. T. Park et al., J. Am. Chem. Soc. **134** (2012), p. 9146. doi:10.1021/ja304042r
- [6] B. Barwick et al., Nature **462** (2009), p. 902. doi:10.1038/nature08662
- [7] V. A. Lobastov et al., Proc. Natl. Acad. Sci. U.S.A. **102** (2005), p. 7069. doi:10.1073/pnas.0502607102
- [8] A. Feist et al., Ultramicroscopy 176 (2017), p. 63. doi:10.1016/j.ultramic.2016.12.005
- [9] F. Houdellier et al., Ultramicroscopy **186** (2018), p. 128. doi:10.1016/j.ultramic.2017.12.015

- [10] E. J. VandenBussche and D. J. Flannigan, Nano Lett. **19** (2019), p. 6687. doi:10.1021/acs.nanolett.9b03074
- [11] E. J. VandenBussche et al., ACS Omega 5 (2020), p. 31867. doi:10.1021/acsomega.0c04711
- [12] S. Tang et al., Nanoscale Adv. 3 (2021), p. 2787. doi:10.1039/D1NA00167A
- [13] D. J. Flannigan et al., J. Chem. Phys. 157 (2022), 180903. doi:10.1063/5.0128109
- [14] P. K. Olshin et al., Struct. Dyn. 7 (2020), 054304. doi:10.1063/4.0000034
- [15] This material is based upon work supported by the U.S. Department of Energy, Office of Science, Office of Basic Energy Sciences under Award No. DE-SC0018204. This material is based upon work supported by the National Science Foundation under Grant No. DMR-1654318. This work was supported partially by the National Science Foundation through the University of Minnesota MRSEC under Award Number DMR-2011401. Part of this work was carried out in the College of Science and Engineering Characterization Facility, University of Minnesota, which has received capital equipment funding from the NSF through the UMN MRSEC program under Award Number DMR-2011401.